VO$_2$/TiN Plasmonic Thermochromic Smart Coatings for Room-Temperature Applications

Qi Hao,* Wan Li, Huiyan Xu, Jiawei Wang, Yin Yin, Huaiyu Wang, Libo Ma, Fei Ma, Xuchuan Jiang, Oliver G. Schmidt, and Paul K. Chu*

Vanadium dioxide/titanium nitride (VO$_2$/TiN) smart coatings are prepared by hybridizing thermochromic VO$_2$ with plasmonic TiN nanoparticles. The VO$_2$/TiN coatings can control infrared (IR) radiation dynamically in accordance with the ambient temperature and illumination intensity. It blocks IR light under strong illumination at 28 °C but is IR transparent under weak irradiation conditions or at a low temperature of 20 °C. The VO$_2$/TiN coatings exhibit a good integral visible transmittance of up to 51% and excellent IR switching efficiency of 48% at 2000 nm. These unique advantages make VO$_2$/TiN promising as smart energy-saving windows.

Thermochromic smart coatings can intelligently control the amount of solar radiation in accordance with the temperature variations.[1] These coatings are designed to block infrared (IR) radiation at a high temperature while allowing it to pass at a low temperature. Vanadium dioxide (VO$_2$) is one of the promising thermochromic materials due to its reversible phase transition and high efficiency in modulating IR transmittance.[2] However, the high transition temperature at 68 °C has hampered room-temperature applications. Although much effort has been made to lower the transition temperature by reducing the grain sizes,[3] introducing elemental doping[4] and adopting appropriate substrates,[5] these strategies lead to sample instability or undesired variations in the spectral response.

Herein, we propose integrating VO$_2$ with titanium nitride (TiN) plasmonic nanoparticles to form a smart coating for room-temperature applications. Plasmonic materials refer to nanostructures that can provide strongly confined charge density oscillations to boost the light–matter interactions in the vicinity.[6] These materials can strongly concentrate light within a nanoscale confined volume and generate heat by ohmic losses when the irradiation wavelength coincides with the plasmon resonant wavelength.[7] TiN is a new-generation refractory plasmonic material with low cost and outstanding thermal and chemical stability.[8] It is highly efficient in absorbing near infrared (NIR) radiation to provide local heating for the surroundings[9] and the efficiency is comparable to or even higher than that of traditional metallic plasmonic materials.[10] Particularly, TiN materials possess low scattering and reflection in the visible light region thus boding well for window coatings. Nevertheless, TiN has not been widely applied to plasmonic applications because its refractory characteristics bring difficulties in sample preparation but nitridation of TiO$_x$ films has been demonstrated to efficiently produce crystal TiN materials.[11] Here, we demonstrate the fabrication of centimeter-scale-patterned TiN nanoparticle arrays by a combination of nanotemplate technique and direct nitridation of the titanium oxide nanoparticles. The TiN nanoparticles inherit the ideal hexagonal superlattice structure from the nanotemplate and exhibit intense plasmonic absorption in the NIR region. The TiN nanoparticles are coated with a pure monoclinic phase (M-phase) VO$_2$ thermochromic film prepared by annealing after physical vapor deposition. In this VO$_2$/TiN hybrid system, the TiN particles convert NIR radiation to heat and accelerate the phase transition in VO$_2$. Different from the pure VO$_2$ thermochromic materials, this hybrid coating

Dr. Q. Hao, W. Li, H. Y. Xu, Prof. F. Ma, Prof. P. K. Chu
Department of Physics and Materials Science
City University of Hong Kong
Tat Chee Avenue, Kowloon 999077, Hong Kong, China
E-mail: haoqihq@163.com; paul.chu@cityu.edu.hk
Dr. Q. Hao, Dr. J. Wang, Dr. Y. Yin, Dr. L. Ma, Prof. O. G. Schmidt
Institute for Integrative Nanosciences
Leibniz IFW Dresden
Helmholtzstraße 20, 01069 Dresden, Germany
H. Y. Xu, Prof. F. Ma
State Key Laboratory for Mechanical Behavior of Materials
Xi'an Jiaotong University
Xi'an, 710049 Shaanxi, China

Prof. H. Wang
Center for Biomedical Materials and Interfaces
Shenzhen Institutes of Advanced Technology
Chinese Academy of Sciences
Shenzhen 518055, P.R. China
Prof. X. Jiang
Department of Chemical Engineering
Monash University
Clayton, VIC 3800, Australia
Prof. O. G. Schmidt
Material Systems for Nanoelectronics
Chemnitz University of Technology
Reichenhainer Str. 70, 09107 Chemnitz, Germany

controls the IR transmittance dynamically in accordance with the ambient temperature and illumination intensity. The VO_2/TiN coating blocks IR radiation at 28 °C depending on the radiation intensity but is IR transparent at 20 °C. Meanwhile, the VO_2/TiN coating exhibits a good integral visible transmittance (380–760 nm) of up to 51% while maintaining excellent NIR switching efficiency of 48% at 2000 nm.
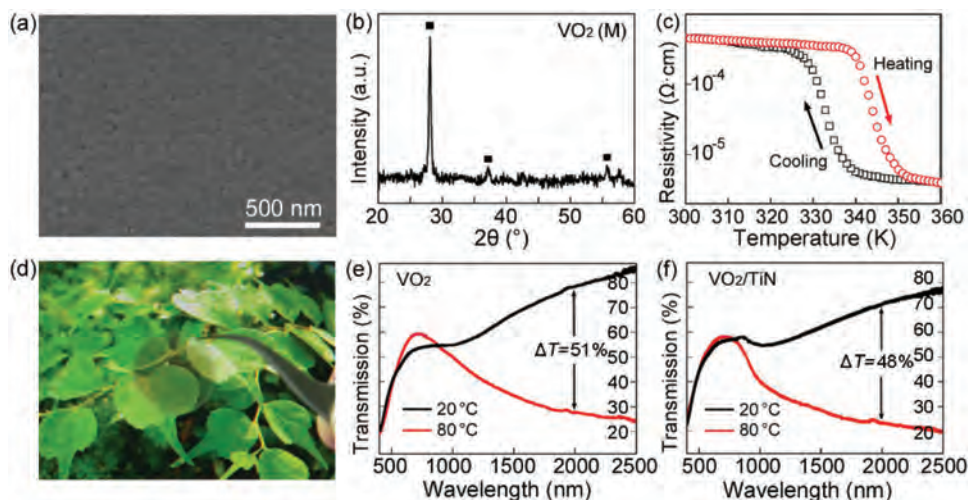
The centimeter-scale TiN plasmonic nanoarray is produced by direct nitridation of titanium oxide (TiO_x) nanoparticles. The patterned TiO_x nanoparticles are fabricated on silicon wafer/quartz substrates by electron-beam evaporation of titanium through an anodic aluminum oxide (AAO) nanomask. This technique allows high-precision wafer-scale fabrication of patterned nanoarrays.[12] The scanning electron micrograph (SEM) image in **Figure 1**a shows the patterned TiO_x nanoparticles with more than 98% coverage. Afterward, nitridation of TiO_x is performed in ammonia at 850 °C for 10 h. Figure 1b,c compares the morphology of the nanoparticles before and after nitridation. Owing to the outstanding thermal stability, the TiN nanoarray inherits the hexagonal patterns from TiO_x after annealing and the particle diameter and interparticle gap are 70 and 30 nm, respectively. Figure 1d presents the X-ray photoelectron spectroscopy (XPS) spectra of the Ti 2p core level as a function of nitridation time. The TiO_x Ti 2p spectrum is composed of two major peaks at 458.8 and 464.3 eV. During nitridation,

these two peaks shift and eventually disappear while new peaks evolve at 455.6 and 461.3 eV corresponding to the TiN Ti $2p_{3/2}$ and Ti $2p_{1/2}$ spin orbital components, respectively. The O 1s and N 1s spectra are shown in Figure S1 in the Supporting Information. Figure 1e shows the X-ray diffraction (XRD) patterns of the samples for different nitridation time. When the nitridation time is 2 h, a small amount of TiN with characteristic peaks at 36.9°, 43.2°, and 62.4° coexists with rutile TiO_2. The TiO_2 phase disappears when the nitridation time is prolonged to 10 h, indicating that pure cubic-phase TiN nanoparticles are produced. The XPS and XRD results are inconsistent with previous reports,[13] demonstrating that plasmonic TiN nanoarrays are successfully fabricated by nitridation of TiO_x. The evolution of the UV–vis spectra of the samples during nitridation is presented in Figure 1f. Strong absorption in the NIR range is observed from the pure TiN nanoparticles, indicating intense plasmon resonances.

Fabrication of vanadium dioxide is performed by magnetron sputtering of vanadium in a mixed ambient of argon and oxygen to produce VO_x films on silicon/quartz. The VO_x composite is annealed in a low-pressure air atmosphere to form the VO_2 crystal. **Figure 2**a shows the annealed VO_2 film and protuberance nanostructures with clearly defined grain boundaries and microcracks. This specific structure facilitates visible transmittance and enhances the optical properties of VO_2 films.[14]
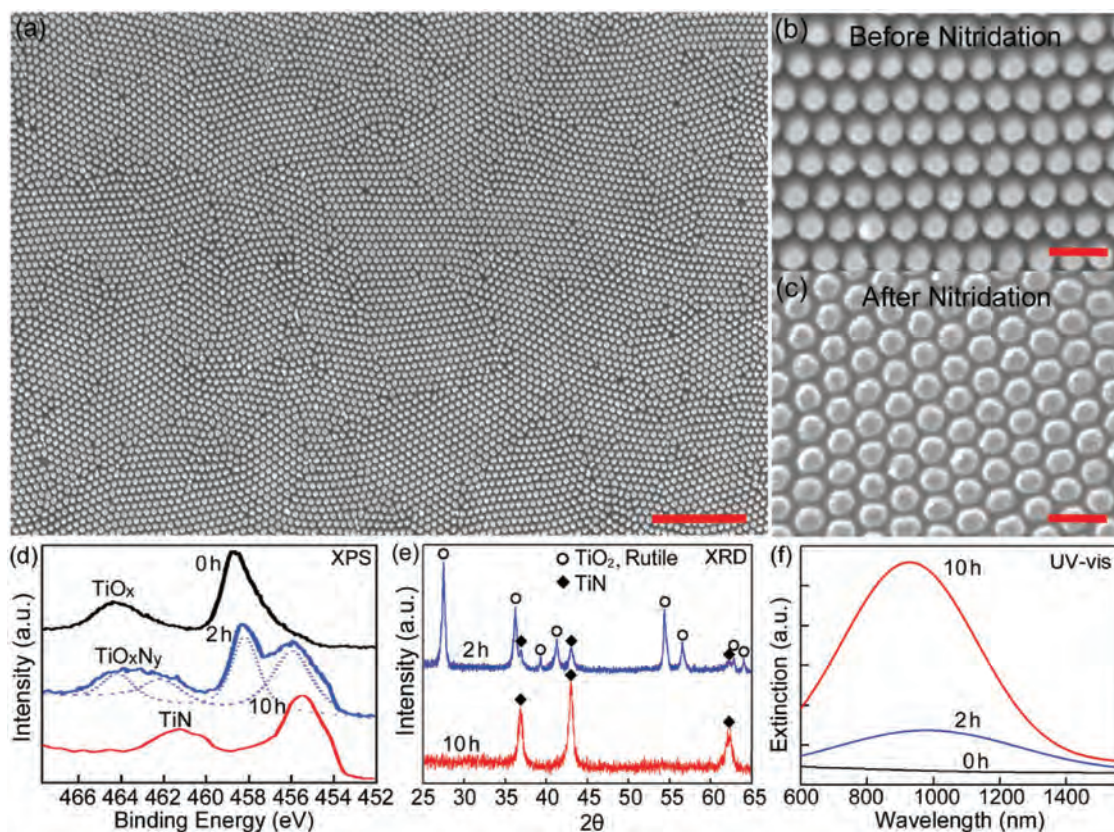
Figure 1. a) Large-area SEM image of the patterned TiO_x nanoparticles fabricated by evaporation through an anodic aluminum oxide mask with the scale bar being 1 μm. b,c) High-resolution SEM images of the nanoparticle arrays before and after nitridation in ammonia at 850 °C with the scale bars being 200 nm. d) XPS spectra and corresponding fitting lines taken in the Ti 2p core-level region from the TiO_x, TiO_xN_y, and TiN nanoarrays with nitridation time of 0, 2, and 10 h, respectively. e) XRD patterns of the TiO_xN_y and TiN samples after nitridation for 2 and 10 h, respectively. f) UV–vis spectra of the TiO_x, TiO_xN_y, and TiN nanoarrays on quartz substrates.

**ADVANCED
SCIENCE NEWS**

www.advancedsciencenews.com

**ADVANCED
MATERIALS**

www.advmat.de

Figure 2. a) SEM image of the annealed VO_2 film on TiN nanoparticles with protuberance structures. b) XRD pattern of the VO_2 crystal. c) Thermal hysteresis loop of electrical resistivity from the VO_2/TiN film. d) Optical photo of the VO_2/TiN coating on quartz. e,f) Transmission spectra of the pure VO_2 and VO_2/TiN coatings at temperatures of 20 °C and 80 °C, respectively, and their corresponding NIR switching efficiencies ΔT at 2000 nm are 51% and 48%, respectively.

Figure 2b reveals the pure monoclinic phase (M-phase) VO_2 with an orientation of $(011)_M$. The monoclinic phase VO_2 possesses a relatively large NIR switching efficiency that can be exploited in smart coating applications. The variation of the electrical resistance of the VO_2 film as a function of temperature for both heating and cooling cycles is plotted in Figure 2c. The characteristic VO_2 transition from the low-temperature semiconducting phase to high-temperature metallic phase is clearly observed in conjunction with a hysteresis loop centered at 60.9 °C with a width of 10.4 °C. This is similar to the switching behavior of pure VO_2, providing evidence that the characteristics of VO_2 are not affected by the TiN nanoparticles. The VO_2 film with a thickness of 50 nm is coated onto the TiN nanoparticles to form the VO_2/TiN hybrid coating. The transmission spectra of the VO_2 and VO_2/TiN samples at 20 and 80 °C, respectively, are compared in Figure 2e,f. Here the transmission spectra are acquired from the backside of the coating. As expected, both exhibit high NIR transmittance at 20 °C following the typical semiconductor behavior and reduced transmittance at 80 °C in the NIR region, which is the characteristic of the metallic state. For architectural smart coatings, the transmittance in the visible range and modulation efficiency in the NIR regions are important. The integral value of the visible transmittance (T_{vis}, 380–780 nm) is obtained from the spectra using the equation

$$X_\rho = \int \varphi_\rho(\lambda) X(\lambda) \, d\lambda / \int \varphi_\rho(\lambda) \, d\lambda \tag{1}$$

where X denotes the transmittance measured by the spectrophotometer. The integral visible transmittances are obtained from the formula $\phi_\rho = \Phi_{lum}$, where Φ_{lum} is equal to the standard luminous efficiency function for photopic vision in the wavelength range of 380–760 nm. The variation in the transmittance before and after the phase transition is defined as the NIR switching efficiency $\Delta T_\lambda = T_\lambda (20\,°C) - T_\lambda (90\,°C)$, where λ is the light wavelength. For the pure VO_2 coating, the calculated values of T_{vis} are 47% and 52% at 20 and 80 °C,

respectively, which are much higher than those of the single-layer VO_2 coating with a similar thickness prepared by magnetron sputtering.[3a] After hybridization with TiN nanoparticles, T_{vis} retains large values of 49% and 51% at 20 °C and 80 °C, respectively. T_{vis} is not significantly reduced after hybridization because the reflection in the visible range is suppressed by TiN nanoparticles.[10b] Furthermore, high ΔT of 51% and 48% at 2000 nm is observed from the VO_2 and VO_2/TiN coatings, respectively, indicating excellent thermochromic properties.

The performance of the VO_2/TiN coating at room temperature is evaluated by using the coating in a double-glass configuration. **Figure 3**a shows the schematic representation of the coating as an intelligent window. The experimental setup is illustrated in Figure 3b, in which IR irradiation at 975 nm is used to excite the TiN nanoparticles and a reference laser at 1550 nm is used to monitor the IR switching efficiency. The wavelength of the IR irradiation is coupled to the TiN plasmonic modes to improve the performance. A sealed double-glass device is designed to reduce thermal convection as shown in Figure 3b. The switching performance of the VO_2/TiN coating at 1550 nm under excitation of 300 mW cm^{-2} at 28 °C is presented in Figure 3c. The transmittance of the coating decreases with irradiation time with a minimum of 30% obtained after 150 s and it recovers in 30 s after the irradiation is turned off. During the measurement, the sample temperature is monitored from the backside of the device with a hand-held infrared thermometer at a maximum of 38 °C.

Figure 3d compares the transition efficiency of the pure VO_2 and VO_2/TiN coatings under 300 mW cm^{-2} IR irradiation for 10 min at 28 °C. For each coating, we define the minimum transmittance in the metallic state as 1.0 and the maximum transmittance in the semiconducting state as zero. This normalized value can be used to evaluate the degree of the phase-transition efficiency in VO_2. The comparison reveals that the transition efficiency of VO_2 is significantly improved when integrated with TiN nanoparticles: a 100% phase transition is observed from the VO_2/TiN coating under excitation of 250 mW cm^{-2}

ADVANCED
SCIENCE NEWS

www.advancedsciencenews.com

ADVANCED
MATERIALS

www.advmat.de
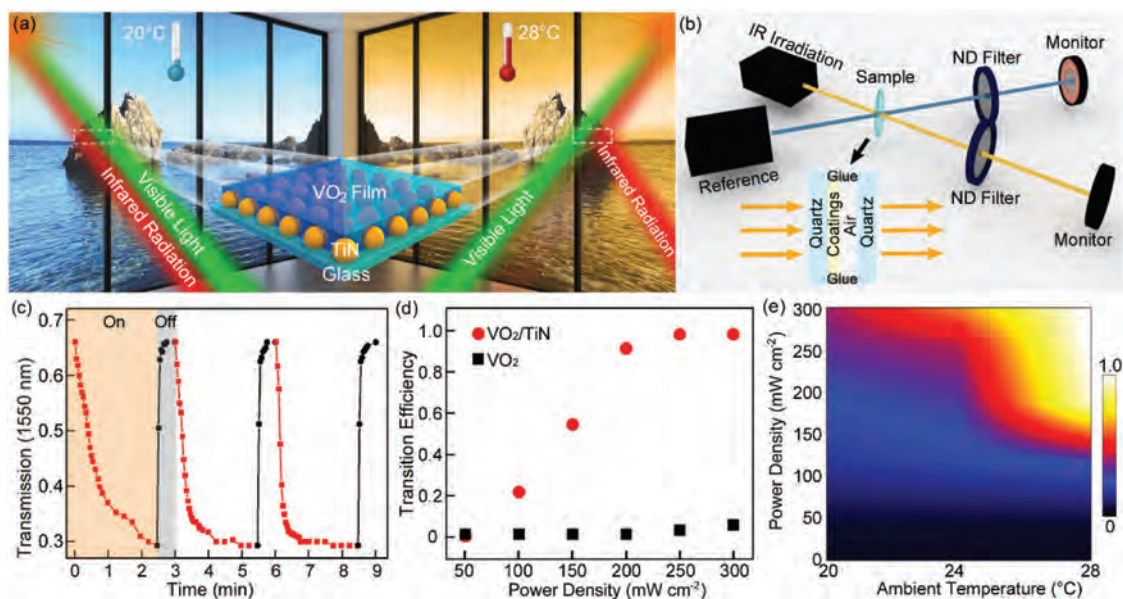
Figure 3. a) Schematic representation of hybrid VO_2/TiN material applied as an intelligent window coating. b) Experimental setup for the measurement and configuration of the double-glass device. An IR irradiation source at 975 nm is used to excite the plasmonic TiN particles and a reference laser at 1550 nm is used to evaluate the IR transmittance efficiency. c) IR switching characteristics of the VO_2/TiN coating under excitation of 300 mW cm^{-2} at 28 °C and 1550 nm. d) Phase-transition efficiency of the pure VO_2 and VO_2/TiN coatings under excitation of 300 mW cm^{-2} at 28 °C. e) 2D map of the transition efficiency in variation with IR radiation intensity and ambient temperature.

while there is only a slight change for pure VO_2 under similar excitation conditions. This slight variation for pure VO_2 may arise from thermal effects or photoinduced phase transition. It has been reported that strong pulse lasers can be used to trigger the phase transition and track the electron and phonon lattice in VO_2.[15] However, light-induced transition is not obvious in our experiments probably due to the different laser intensities. It should be noted that the 975 nm IR irradiation source is adopted in the experiment to couple with the plasmon resonance profile of the TiN nanoparticles (Figure 1f), which is crucial to optimize the transition efficiency. The efficiency is pared significantly if the wavelength of the IR irradiation is out of the plasmon resonance region (see Figure S2, Supporting Information). Figure 3e shows the transition efficiency of the VO_2/TiN coating in response to the ambient temperature and irradiation power density. The VO_2/TiN coating blocks up to 70% of the IR radiation at 28 °C depending on the radiation intensity and allows most of it to pass through at 20 °C. The results clearly show that the VO_2/TiN coating controls the IR transmittance dynamically according to the ambient temperature and irradiation intensity.

In conclusion, we demonstrate that the VO_2/TiN coating can intelligently control the IR transmittance depending on the irradiation intensity and ambient temperature. The centimeter-scale TiN plasmonic nanoarray is fabricated by nanomask-assisted evaporation in combination with direct nitridation of TiO_x nanoparticles. The TiN nanoparticles are coated with a pure monoclinic phase (M-phase) VO_2 film to produce the VO_2/TiN coating. When properly excited by illumination, the VO_2/TiN smart coating blocks 70% of the IR radiation at 28 °C while showing good IR transparency at 20 °C. More importantly, the VO_2/TiN coating exhibits a good integral visible transmittance

of up to 51% and excellent NIR switching efficiency of 48% at 2000 nm. These advantages make VO_2/TiN promising as smart coatings for room-temperature applications. The thermochromic performance can be further improved by introducing elemental doping, optimizing the plasmonic spectrum, and using thermal insulation coatings to reduce convection.

Experimental Section

Fabrication of TiN Nanoparticles: The AAO nanomask was fabricated by anodizing aluminum films in an oxalic acid solution and transferred onto silicon or quartz substrates for evaporation. The pore diameter and interpore distance of the mask were 65 and 100 nm, respectively. More details about the fabrication and optimization of the AAO mask can be found from our previous publication. Titanium was evaporated through the mask in an oxygen atmosphere at 1.0×10^{-2} Pa to produce TiO_x nanoparticles at a deposition rate of 0.2 nm s^{-1} and the film thickness was 25 nm. After deposition, the AAO mask was peeled from the substrate with a tape and the TiO_x nanoparticles were nitrided in gaseous ammonia (99.99%) at 850 °C for 10 h. Argon was used as a protective gas during the cooling process.

Fabrication of VO_2 Films: The VO_x composite was sputtered onto the TiN nanoparticles in a mixed ambient of oxygen and argon (1:3) at 3×10^{-3} Pa and 20 °C. The VO_x/TiN film was annealed at 500 °C for 10 min at 100 Pa with a heating rate of 10 °C min^{-1} and then cooled naturally inside the equipment. More details about the synthesis of the high-performance VO_2 are available in our previous publication.[16] It should be noted that the TiN nanoparticles were not oxidized during annealing (Figure S3, Supporting Information).

Optical Measurement: A 975 nm laser diode (Thorlabs) was used as the IR irradiation source and a 1550 nm laser (Yenista optics, T100) was used as the reference laser. The reference laser power was maintained at 30 mW cm^{-2} during the measurement. The lasers were focused to a spot size of 2 mm and a power meter (FieldMaxII-TO) was used to monitor the laser intensity. The sample temperature was monitored

**ADVANCED
SCIENCE NEWS**

www.advancedsciencenews.com

**ADVANCED
MATERIALS**

www.advmat.de

by a hand-held infrared thermometer from the backside of the double-glass device. The JGS3 quartz glass for infrared research was used as the sample substrate for VO$_2$/TiN coating in the optical measurement and the transmission spectrum for JGS3 is displayed in Figure S4 in the Supporting Information. The VO$_2$/TiN coating on quartz was sealed on the inner side of a double-glass device to reduce thermal convection. The double-glass device was fabricated by gluing the edge of the sample substrate to another quartz glass sheet (glue from UHU PLUS). The laser beam passed through the sample from the backside of the coating during the optical measurement, and in this way the laser interacted with the TiN nanoparticles prior to the VO$_2$ coating, otherwise, the efficiency would be suppressed greatly due to IR reflection from the VO$_2$ coating (see Figure S5 in the Supporting Information).

Characterization: The morphology and properties of the samples were assessed by SEM (JEOL JSM-820), XRD (Bruker AXS D2 Phaser and Rigaku, Smartlab 3) with a Cu Kα X-ray source, UV–vis spectrophotometry (LAMBDA750), XPS (ESCALB MK-II, VG Instruments) using Al Kα radiation and physical property measurement system (PPMS, Quantum Design PPMS-9). The electrical resistivity was measured by the four-electrode method at a heating and cooling rate of 1 K min^{-1}.

Supporting Information

Supporting Information is available from the Wiley Online Library or from the author.

Conflict of Interest

The authors declare no conflict of interest.

[1] M. Kamalisarvestani, R. Saidur, S. Mekhilef, F. Javadi, *Renewable Sustainable Energy Rev.* **2013**, *26*, 353.

[2] a) Y. Gao, H. Luo, Z. Zhang, L. Kang, Z. Chen, J. Du, M. Kanehira, C. Cao, *Nano Energy* **2012**, *1*, 221; b) N. B. Aetukuri, A. X. Gray, M. Drouard, M. Cossale, L. Gao, A. H. Reid, R. Kukreja, H. Ohldag, C. A. Jenkins, E. Arenholz, *Nat. Phys.* **2013**, *9*, 661; c) Z. Chen, Y. Gao, L. Kang, C. Cao, S. Chen, H. Luo, *J. Mater. Chem. A* **2014**, *2*, 2718; d) S. Wang, M. Liu, L. Kong, Y. Long, X. Jiang, A. Yu, *Prog. Mater. Sci.* **2016**, *81*, 1; e) M. Liu, B. Su, Y. V. Kaneti, Z. Chen, Y. Tang, Y. Yuan, Y. Gao, L. Jiang, X. Jiang, A. Yu, *ACS Nano* **2016**, *11*, 407; f) Y. Ke, X. Wen, D. Zhao, R. Che, Q. Xiong, Y. Long, *ACS Nano* **2017**, *11*, 7542; g) M. Li, S. Magdassi, Y. Gao, Y. Long, *Small* **2017**, *13*, 1701147.

[3] a) D. Brassard, S. Fourmaux, M. Jean-Jacques, J. Kieffer, M. El Khakani, *Appl. Phys. Lett.* **2005**, *87*, 051910; b) Y. Yang, K. Lee, M. Zobel,

[4] M. Mackovic, T. Unruh, E. Spiecker, P. Schmuki, *Adv. Mater.* **2012**, *24*, 1571.

[5] a) R. Binions, C. Piccirillo, R. G. Palgrave, I. P. Parkin, *Chem. Vap. Deposition* **2008**, *14*, 33; b) Y. Gao, C. Cao, L. Dai, H. Luo, M. Kanehira, Y. Ding, Z. L. Wang, *Energy Environ. Sci.* **2012**, *5*, 8708; c) D. Li, M. Li, J. Pan, Y. Luo, H. Wu, Y. Zhang, G. Li, *ACS Appl. Mater. Interfaces* **2014**, *6*, 6555; d) J. T. Zhu, Y. J. Zhou, B. B. Wang, J. Y. Zheng, S. D. Ji, H. L. Yao, H. J. Luo, P. Jin, *ACS Appl. Mater. Interfaces* **2015**, *7*, 27796.

[5] a) Z. Zhang, Y. Gao, H. Luo, L. Kang, Z. Chen, J. Du, M. Kanehira, Y. Zhang, Z. L. Wang, *Energy Environ. Sci.* **2011**, *4*, 4290; b) J. Jeong, N. Aetukuri, T. Graf, T. D. Schladt, M. G. Samant, S. S. P. Parkin, *Science* **2013**, *339*, 1402; c) L. Fan, S. Chen, Z. Luo, Q. Liu, Y. Wu, L. Song, D. Ji, P. Wang, W. Chu, C. Gao, *Nano Lett.* **2014**, *14*, 4036.

[6] a) E. Hutter, J. H. Fendler, *Adv. Mater.* **2004**, *16*, 1685; b) H. A. Atwater, A. Polman, *Nat. Mater.* **2010**, *9*, 205; c) S. Linic, P. Christopher, D. B. Ingram, *Nat. Mater.* **2011**, *10*, 911.

[7] a) J. R. Cole, N. A. Mirin, M. W. Knight, G. P. Goodrich, N. J. Halas, *J. Phys. Chem. C* **2009**, *113*, 12090; b) G. Baffou, R. Quidant, F. J. García de Abajo, *ACS Nano* **2010**, *4*, 709.

[8] a) G. V. Naik, J. Kim, A. Boltasseva, *Opt. Mater. Express* **2011**, *1*, 1090; b) G. V. Naik, J. L. Schroeder, X. J. Ni, A. V. Kildishev, T. D. Sands, A. Boltasseva, *Opt. Mater. Express* **2012**, *2*, 478; c) U. Guler, A. Boltasseva, V. M. Shalaev, *Science* **2014**, *344*, 263; d) A. Comin, L. Manna, *Chem. Soc. Rev.* **2014**, *43*, 3957; e) U. Guler, V. M. Shalaev, A. Boltasseva, *Mater. Today* **2015**, *18*, 227; f) U. Guler, A. V. Kildishev, A. Boltasseva, V. M. Shalaev, *Faraday Discuss.* **2015**, *178*, 71; g) L. Gui, S. Bagheri, N. Strohfeldt, M. Hentschel, C. M. Zgrabik, B. Metzger, H. Linnenbank, E. L. Hu, H. Giessen, *Nano Lett.* **2016**, *16*, 5708.

[9] a) U. Guler, J. C. Ndukaife, G. V. Naik, A. G. A. Nnanna, A. V. Kildishev, V. M. Shalaev, A. Boltasseva, *Nano Lett.* **2013**, *13*, 6078; b) W. He, K. Ai, C. Jiang, Y. Li, X. Song, L. Lu, *Biomaterials* **2017**, *132*, 37.

[10] a) G. V. Naik, V. M. Shalaev, A. Boltasseva, *Adv. Mater.* **2013**, *25*, 3264; b) W. Li, U. Guler, N. Kinsey, G. V. Naik, A. Boltasseva, J. G. Guan, V. M. Shalaev, A. V. Kildishev, *Adv. Mater.* **2014**, *26*, 7959; c) A. Lalisse, G. Tessier, J. Plain, G. Baffou, *J. Phys. Chem. C* **2015**, *119*, 25518; d) S. Ishii, R. P. Sugavaneshwar, T. Nagao, *J. Phys. Chem. C* **2016**, *120*, 2343.

[11] a) J. Li, L. Gao, J. Sun, Q. Zhang, J. Guo, D. Yan, *J. Am. Ceram. Soc.* **2001**, *84*, 3045; b) S. Prayakarao, S. Robbins, N. Kinsey, A. Boltasseva, V. Shalaev, U. Wiesner, C. Bonner, R. Hussain, N. Noginova, M. Noginov, *Opt. Mater. Express* **2015**, *5*, 1316; c) U. Guler, D. Zemlyanov, J. Kim, Z. Wang, R. Chandrasekar, X. Meng, E. Stach, A. V. Kildishev, V. M. Shalaev, A. Boltasseva, *Adv. Opt. Mater.* **2017**, *5*, 1600717.

[12] a) Q. Hao, H. Huang, X. Fan, X. Hou, Y. Yin, W. Li, L. Si, H. Nan, H. Wang, Y. Mei, T. Qiu, P. K. Chu, *Nanotechnology* **2017**, *28*, 105301; b) Q. Hao, H. Huang, X. Fan, Y. Yin, J. Wang, W. Li, T. Qiu, L. Ma, P. K. Chu, O. G. Schmidt, *ACS Appl. Mater. Interfaces* **2017**, *4*, 36199.

[13] a) N. C. Saha, H. G. Tompkins, *J. Appl. Phys.* **1992**, *72*, 3072; b) E. Galvanetto, F. Galliano, F. Borgioli, U. Bardi, A. Lavacchi, *Thin Solid Films* **2001**, *384*, 223.

[14] Z. Zhang, Y. Gao, Z. Chen, J. Du, C. Cao, L. Kang, H. Luo, *Langmuir* **2010**, *26*, 10738.

[15] a) D. Hilton, R. Prasankumar, S. Fourmaux, A. Cavalleri, D. Brassard, M. El Khakani, J. Kieffer, A. Taylor, R. Averitt, *Phys. Rev. Lett.* **2007**, *99*, 226401; b) M. Liu, M. Wagner, E. Abreu, S. Kittiwatanakul, A. McLeod, Z. Fei, M. Goldflam, S. Dai, M. Fogler, J. Lu, *Phys. Rev. Lett.* **2013**, *111*, 096602; c) B. T. O'Callahan, A. C. Jones, J. H. Park, D. H. Cobden, J. M. Atkin, M. B. Raschke, *Nat. Commun.* **2015**, *6*, 6849; d) S. Lysenko, N. Kumar, A. Rúa, J. Figueroa, J. Lu, F. Fernández, *Phys. Rev. B* **2017**, *96*, 075128.

[16] H. Xu, Y. Huang, S. Liu, K. Xu, F. Ma, P. K. Chu, *RSC Adv.* **2016**, *6*, 79383.

ADVANCED MATERIALS

Supporting Information

VO$_2$/TiN Plasmonic Thermochromic Smart Coatings for Room-Temperature Applications

Qi Hao,* Wan Li, Huiyan Xu, Jiawei Wang, Yin Yin, Huaiyu Wang, Libo Ma, Fei Ma, Xuchuan Jiang, Oliver G. Schmidt, and Paul K. Chu*

Supporting Information

VO₂/TiN plasmonic thermochromic smart coatings for room-temperature applications

Qi Hao*, Wan Li, Huiyan Xu, Jiawei Wang, Yin Yin, Huaiyu Wang, Libo Ma, Fei Ma,

Xuchuan Jiang, Oliver G. Schmidt and Paul K. Chu*

Dr. Q. Hao, W. Li, H. Y. Xu, Prof. F. Ma, and Prof. P. K. Chu
Department of Physics and Materials Science, City University of Hong Kong, Tat Chee
Avenue, Kowloon, Hong Kong, China
E-mail: haoqihq@163.com (Q. H.)
E-mail: paul.chu@cityu.edu.hk (P. K. C.)

Dr. Q. Hao, Dr. J. Wang, Dr. Y. Yin, Dr. L. Ma and Prof. O. G. Schmidt
Institute for Integrative Nanosciences, Leibniz IFW Dresden, Helmholtzstraße 20, 01069
Dresden, Germany

H. Y. Xu, and Prof F. Ma
State Key Laboratory for Mechanical Behavior of Materials, Xi'an Jiaotong University, Xi'an
710049, Shaanxi, China

Prof. H. Wang
Center for Biomedical Materials and Interfaces, Shenzhen Institutes of Advanced Technology,
Chinese Academy of Sciences, Shenzhen 518055, Guangdong, China

Prof. X. Jiang
Department of Chemical Engineering, Monash University, Clayton, VIC 3800, Australia

Prof. O. G. Schmidt
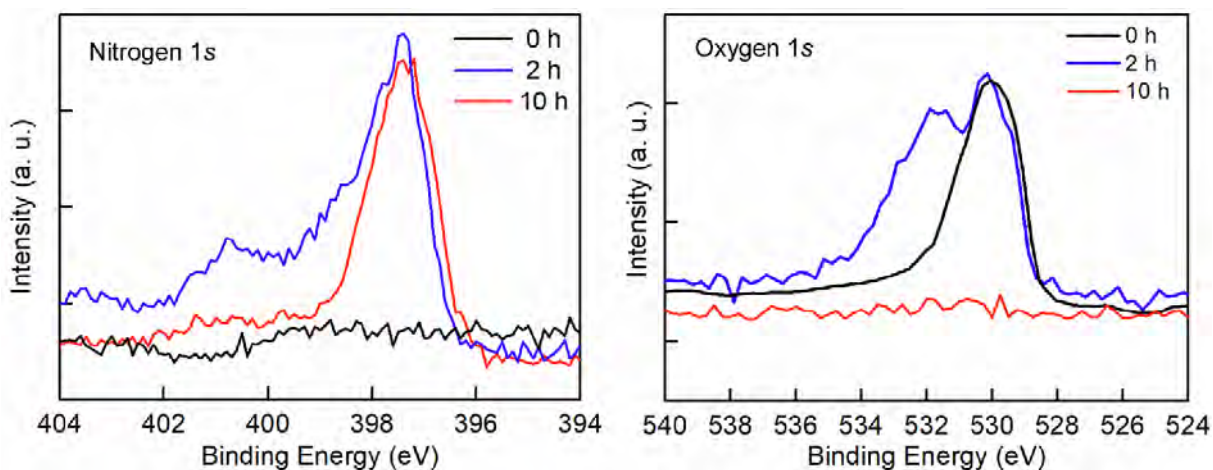Material Systems for Nanoelectronics, Chemnitz University of Technology, Reichenhainer
Str. 70, 09107 Chemnitz, Germany

Figure S1. N 1s and O 1s XPS spectra acquired from the TiO_x, TiO_xN_y and TiN samples after nitridation for 0 h, 2 h, and 10 h. The major nitrogen peak at 397.3 eV is observed for both the TiN and TiO_xN_y samples. A shoulder peak at about 399 eV and another peak at about 401 eV are observed from TiO_xN_y possibly due to oxynitride. The major oxygen peak of TiO_x and TiO_xN_y is located at 530.2 eV and another peak at 531.6 eV observed from TiO_xN_y may arise from sub-stoichiometric oxide.[1]

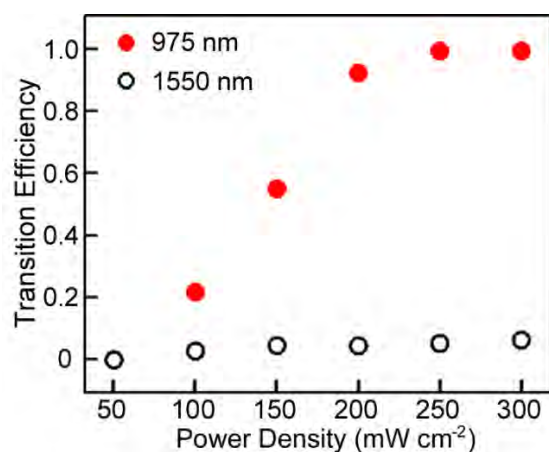[1]   N. C. Saha, H. G. Tompkins, *J. Appl. Phys.* **1992**, *72*, 3072.

Figure S2. Phase transition efficiency of the VO_2/TiN coating in response to different IR power densities under IR irradiation at 975 nm and 1550 nm. The experiments are performed at 28 °C and no obvious changes are observed for a larger laser power density.
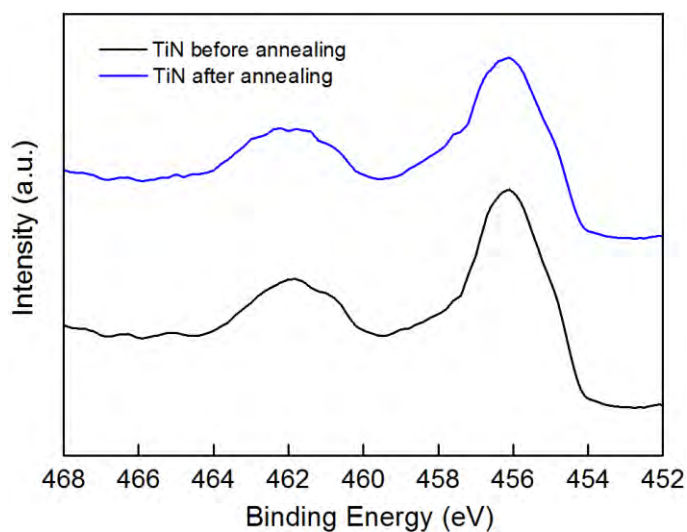

Figure S3. XPS spectra taken in the Ti 2p core-level region from the TiN nanoarray before (black) and after (blue) annealing in vacuum at 100 Pa and 500 °C for 10 min. The annealing parameters are the same as those used in the fabrication of the VO_2 crystal. The comparison shows that the TiN nanoparticles are not significantly oxidized during annealing.
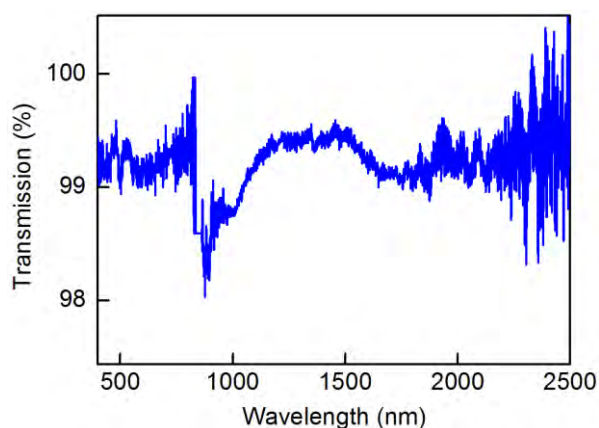
Figure S4. Transmission spectrum of the JGS3 quartz substrate. The quartz glass exhibits good transmittance in the visible and near-infrared regions.
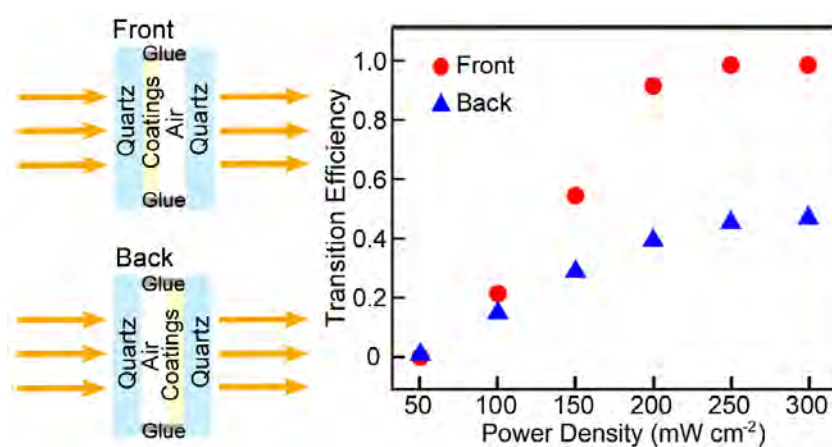

Figure S5. Transition efficiency of the VO_2/TiN coating sealed in a double glass device with IR irradiation passing through from the front and backside. The comparison shows that the efficiency is much higher when the laser interacts with the TiN nanoparticles prior to the VO_2 coating. This is because VO_2 reflects the IR irradiation and reflection from the backside is suppressed by the TiN nanoparticles. Similar results have been observed from the VO_2/TiN coating without a double glass device using an IR laser with a larger intensity.